RAPID COMMUNICATION

Prediction of $LiCrTe_2$ monolayer as a half-metallic ferromagnet with a high Curie temperature

Li-Man Xiao(肖丽蔓), Huan-Cheng Yang(杨焕成)[†], and Zhong-Yi Lu(卢仲毅)[‡]

Department of Physics and Beijing Key Laboratory of Opto-electronic Functional Materials & Micro-nano Devices, Renmin University of China, Beijing 100872, *China*

(Received 7 December 2022; revised manuscript received 4 February 2023; accepted manuscript online 23 February 2023)

By using first-principles electronic structure calculations, we predict a new two-dimensional half-metallic ferromagnet (2DHMF) with distorted square structure, i.e., the $LiCrTe_2$ monolayer. The results show that the $LiCrTe_2$ monolayer is dynamically, thermally, and mechanically stable, and takes a large in-plane magnetic anisotropy, a wide spin gap, a large magnetization, and a very high Curie temperature. Under a biaxial strain ranging from -5% to $+5\%$, the ferromagnetism, half-metallicity, and high Curie temperature are maintained well. Both tensile and compressive strains can significantly increase the magnitude of the magnetocrystalline anisotropy energy (MAE) and a transition from in-plane easy-$x(y)$-axis to out-of-plane easy-z-axis occurs when the compressive strain exceeds 1%. Our systematic study of the $LiCrTe_2$ monolayer enables its promising applications in spintronics.

Keywords: two-dimensional half-metallic ferromagnet, electronic structures, first-principles calculations

PACS: 75.70.Ak, 73.22.–f **DOI:** 10.1088/1674-1056/acbe2e

1. Introduction

Spintronics offers great opportunities to develop high speed, low power, and high integration density electronic devices and it is also one of the most promising next generation information technologies.[1,2] Different from traditional electronics, which takes full advantage of the electron's charge degree of freedom, spintronics is devoted to incorporating the electron's spin degree of freedom. Therefore, it is important to generate spin-polarised electrons in traditional nonmagnetic semiconductor materials. One of the most common methods is spin injection from a ferromagnetic (FM) material, e.g., conventional FM metals (Fe, Co, and Ni), FM semiconductors, and half-metallic ferromagnets (HMFs) (behaving as a metal in one spin channel and as a semiconductor or insulator in the other spin channel). Among them, FM semiconductors and HMFs are more suitable as spin injection materials because they can intrinsically provide single spin channel electrons with the spin polarization reaching 100%, which can effectively improve the spin injection efficiency.[1]

Compared to bulk FM semiconductors and HMFs, two dimensional FM semiconductors and HMFs can not only provide up to 100% spin-polarized current but also possess novel electronic, mechanical, optical, and magnetic properties, especially take advantages of straightforward integration into heterostructural devices. However, presently demonstrated two dimensional FM semiconductors still show rather low Curie temperature (T_c) due to rather weak ferromagnetic couplings among the magnetic ions (45 K for CrI_3 monolayer[3] and 30 K for bilayer $Cr_2Ge_2Te_6$[4]), far from room temperature for practical applications. On the other hand, one may be aware that 2DHMFs usually exhibit a much higher T_c due to the strong exchange interaction driven by charge carriers, such as 768 K for h-VN,[5] 730 K for h-CrC,[6] and 495 K for MnP.[7] Besides a high Curie temperature, a wide half-metallic gap (E_g) and a large magnetic anisotropy are also important for ideal HMFs. The half-metallic gap should be wide enough to prevent the spin-flip transition caused by the thermal excitation and preserve the half-metallicity of HMFs at room temperature. The magnetocrystalline anisotropy is fundamentally critical to give rise to long-range magnetic ordering in 2D materials on one hand and it is also important for improving spin injection efficiency on the other hand. In addition, a large magnetization is also required to improve the spin injection rate. Therefore, it is of fundamental interest to discover new 2DHMFs with sizable magnetocrystalline anisotropy energy (MAE), wide E_g, large magnetization, and high Curie temperature.

In this work, we propose a 2D intrinsic HMF, the $LiCrTe_2$ monolayer, with significant magnetocrystalline anisotropy, wide spin gap, large magnetization, and high Curie temperature. We study systematically the structure, electronic, and magnetic properties of the $LiCrTe_2$ monolayer by using first-principles electronic structure calculations.

[†]Corresponding author. E-mail: hcyang@ruc.edu.cn
[‡]Corresponding author. E-mail: zlu@ruc.edu.cn

© 2023 Chinese Physical Society and IOP Publishing Ltd

2. Computational methods

The first-principles electronic structure calculations were performed in the framework of density functional theory (DFT) using the Vienna *Ab-initio* Simulation Package (VASP).[8,9] The generalized gradient approximation (GGA) of Perdew–Burke–Ernzerhof (PBE) type was adopted for the exchange–correlation functional.[10] The projector augmented wave (PAW) method[11,12] was adopted to describe the interactions between valence electrons and nuclei. The kinetic energy cutoff of the plane-wave basis was set to be 650 eV. The total energy convergence and the atomic force tolerance were set to be 10^{-6} eV and 0.01 eV/Å, respectively. For describing the Fermi–Dirac distribution function, a Gaussian smearing of 0.02 eV was used. The $8\times8\times1$, $4\times4\times1$ and $2\times2\times1$ gamma-centered Monkhorst–Pack grids[13] were used for the Brillouin zone (BZ) sampling of the primitive cell, the $2\times2\times1$ supercell and the $4\times4\times1$ supercell, respectively. We adopted a vacuum distance about 20 Å in the c direction to eliminate the interactions between adjacent layers in the slab modeling the two-dimensional systems. To account for the correlation effects of Cr 3d orbitals, we also performed GGA+U calculations by using the simplified rotationally invariant version of Dudarev *et al.*[14] The $U_{\rm eff}$ was set to 3 eV, $U_{\rm eff}=3.5$ eV and 4 eV were also used to calculate the electronic structures and magnetic properties as in the previous work[15] (ferromagnetic semiconductor $LiCrTe_2$ monolayer with $P3m1$ space group). For the MAE calculation, the spin–orbit coupling (SOC) was included. The phonon spectra was additionally simulated by PHONOPY[16] and the force constants were calculated based on the density functional perturbation theory with a $4\times4\times1$ supercell. Based on Nosé–Hoover thermostat scheme,[17] the *ab initio* molecular dynamics (AIMD) simulations were conducted in the NVT ensemble up to 15 ps with a time step of 3.0 fs at 300 K by using a $3\times3\times1$ supercell. The Monte Carlo simulations based on the classical Heisenberg model were employed to describe the thermal dynamics of magnetism in equilibrium state,[18,19] for which the open source project MCSOLVER code was used.[20]

3. Results and discussion

3.1. Crystal structure and stability

The optimized geometric configuration of $LiCrTe_2$ monolayer with space group $P\bar{4}2_1m$ (#113) is displayed in Figs. 1(a) and 1(b). The $LiCrTe_2$ monolayer takes a fivefold layered structure, i.e., Te–Li–Cr–Li–Te. The primitive cell contains two Li, two Cr, and four Te atoms, in which the Cr atoms, the upper Li atoms and the lower Li atoms form a tetragonal lattice. Each Cr atom is located at the center of a compressed tetrahedron field formed by four Te atoms. Structurally, the $LiCrTe_2$ monolayer is similar to the FeSe monolayer.[21] After full relaxation, the lattice parameter of the $LiCrTe_2$ monolayer is $a=6.376$ Å. The Cr–Te bond length is 2.65 Å and the Li–Te bond length is either 2.72 Å or 2.75 Å as shown in Fig. 1(a). The bond angles for Te–Cr–Te are either 104.8° or 119.2° and for Te–Li–Te are 85.2° or 100.2° or 152.2° (see Figs. 1(a) and 1(b)). The bond angle for Cr–Te–Cr is 116.7°.

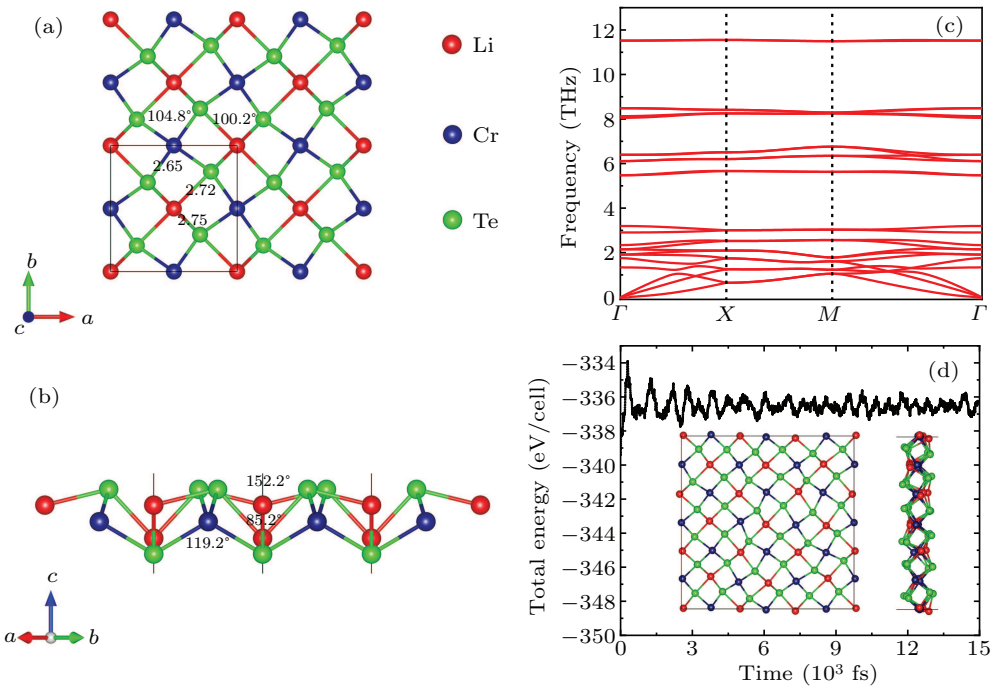


Fig. 1. Crystal structure of the $LiCrTe_2$ monolayer: (a) top view and (b) side view. (c) The calculated phonon spectrum. (d) The fluctuation of total energy of the $LiCrTe_2$ monolayer and the snapshot for the final configuration after AIMD simulation at 300 K.

To testify its stability, we studied the lattice dynamics, thermaldymics, and mechanical properties of the $LiCrTe_2$ monolayer. The lattice dynamics was studied by using PHONOPY and the calculated phonon spectrum is shown in Fig. 1(c). No imaginary frequency is found in the phonon dispersion, confirming the dynamical stability of the $LiCrTe_2$ monolayer. Figure 1(d) displays the evolution of the total energy over the 15 ps simulation time at 300 K with the top and side view snapshots of the structure at 15 ps after the AIMD simulation. There is no structural destruction and the 2D planar networks are well maintained, which indicates that all atoms in the cell vibrate near their equilibrium positions and thus the $LiCrTe_2$ monolayer is thermally stable. Furthermore, the time-dependent total energy shows small fluctuation, further suggesting the thermal stability of the $LiCrTe_2$ monolayer. The calculated elastic constants of the $LiCrTe_2$ monolayer are $C_{11} = 20.012$ N/m, $C_{12} = 3.133$ N/m and $C_{66} = 9.571$ N/m, which satisfy well the mechanical stability condition, $C_{11} > 0$, $C_{66} > 0$ and $C_{11} > |C_{12}|$,[22] indicating that it is mechanically stable. Moreover, for a stable 2D monolayer, it must hold its own weight and geometry. The gravity induced out-of-plane deformation can be estimated as[23]

$$\frac{h}{L} \approx \left(\frac{\rho g L}{Y_{2D}}\right)^{\frac{1}{3}},$$

where $\rho = 2.567 \times 10^{-6}$ kg/m^2 is the 2D mass density, L is the edge length of the flak, and Y_{2D} is the 2D Young's modulus. Due to the C_4 rotation symmetry of the $LiCrTe_2$ structure, the calculated direction-dependent Young's modulus (Y_{2D}) has the C_4 symmetry with values from 19.521 N/m to 20.954 N/m, as shown in Fig. 2. For a typical value $L = 100$ μm, the calculated h/L is between 4.93×10^{-4} and 5.05×10^{-4}, comparable to that of $CrCl_3$ (4.65×10^{-4} [24]) and $CrGeTe_3$ (5×10^{-4} [25]), and is of the same order of magnitude as that of graphene,[23] suggesting that the $LiCrTe_2$ monolayer is able to keep its free-standing plane structure under its own weight without substrate.

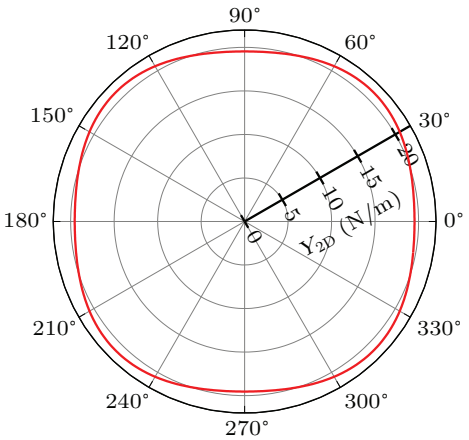


Fig. 2. The angular dependence of Young's modulus Y_{2D} in units of N/m.

3.2. Magnetic and electronic properties

In order to determine the magnetic ground state of the $LiCrTe_2$ monolayer, all possible antiferromagnetic configurations (six ones within a $2 \times 2 \times 1$ supercell) and one ferromagnetic configuration are considered. The six AFM configurations are shown in Fig. 3. Among these seven magnetic configurations, the calculation results show that the FM state takes the lowest energy, thus being the ground state. The energy differences of the six AFM states with respect to the FM state ($\Delta E = E_{AFM} - E_{FM}$), with different $U_{eff} = 3$ eV, 3.5 eV, and 4 eV, are shown in Fig. 4. The AFM6 configuration takes the hightest energy, which is about 487 meV/Cr larger than that of the FM configuration. The total magnetization of the $LiCrTe_2$ monolayer is about 6 μ_B per primitive cell. The magnetism is mainly from the Cr atoms, whose magnetic moments are about 3.6 μ_B per Cr atom, while the Te atoms take small opposite magnetic moment (-0.3 μ_B per Te atom) and the magnetic moments on the Li atoms are negligible as shown in the spin density distribution (Fig. 5(a)). As shown in Fig. 6(a), almost only the majority spin channels of the Cr-3d orbitals are occupied, resulting in a magnetic moment of about 4 μ_B on each Cr atom. The magnetic moments

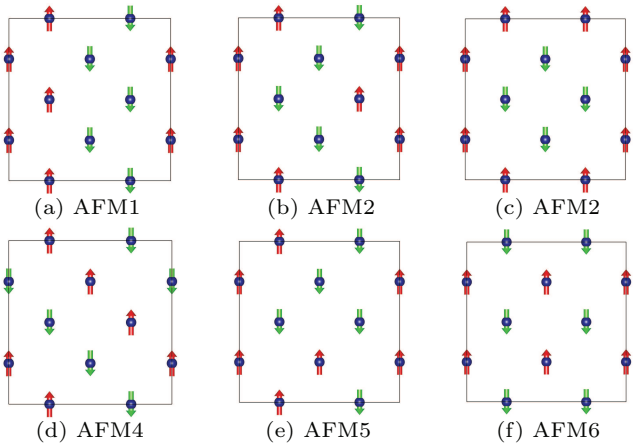


Fig. 3. Top view of six AFM magnetic configurations. Only Cr atoms are shown for simplicity. The $2 \times 2 \times 1$ supercell is outlined by solid black lines. The red arrows represent up-spins and the green arrows represent down-spins.

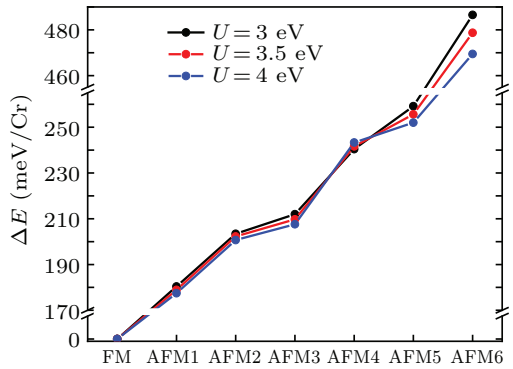


Fig. 4. The energy differences of the AFM states with respect to the FM state, i.e., $\Delta E = E_{AFM} - E_{FM}$.

on the Te atoms are mainly from the polarization of their p orbitals due to the p–d hybridization (see Fig. 6(a)) between the Te and Cr atoms.

The MAEs are calculated to be 0.281 meV/f.u., 0.407 meV/f.u., and 0.620 meV/f.u. for $U_{\rm eff} = 3$ eV, 3.5 eV, and 4 eV, respectively, which are in the same order of many 2D magnents[26] and significantly larger than those found for commonly used ferromagnetic materials such as bulk Fe (1.4 μeV per atom) and bulk Ni (2.7 μeV per atom).[27] The easy magnetization direction is lying in the plane with the intrinsic easy-axis along x (or along y due to the C_4 rotation symmetry). The xy magnetization direction takes energy about 0.015 meV/Cr higher than that of the intrinsic easy-axis.

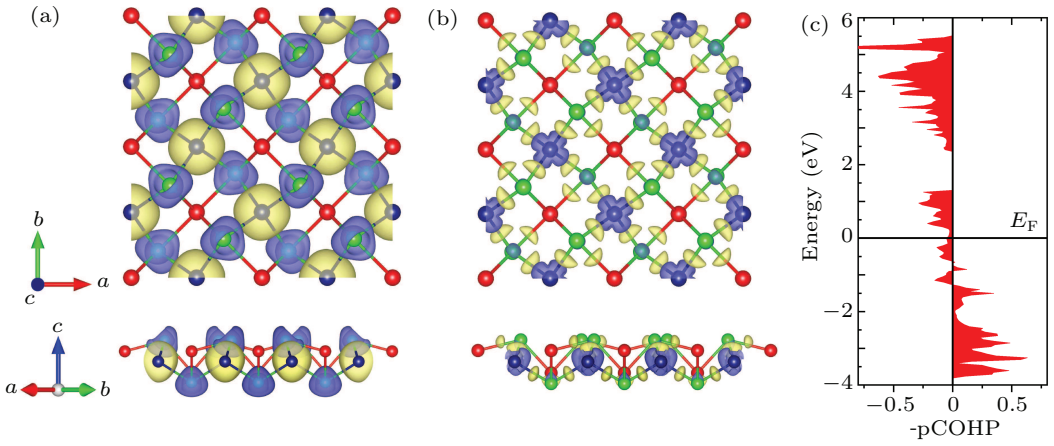


Fig. 5. (a) Top and side views of the spin polarization distribution with the isosurface of 0.006 e/Å^3. The yellow and blue colors indicate the spin-majority and spin-minority polarizations, respectively. (b) Top and side views of the differential charge density, where the yellow and blue regions respectively denote the electron accumulation and depletion with the isosurface being set to 0.008 e/Å^3. (c) Crystal orbital Hamilton population (COHP) analysis projected on the Cr–Te bonds.

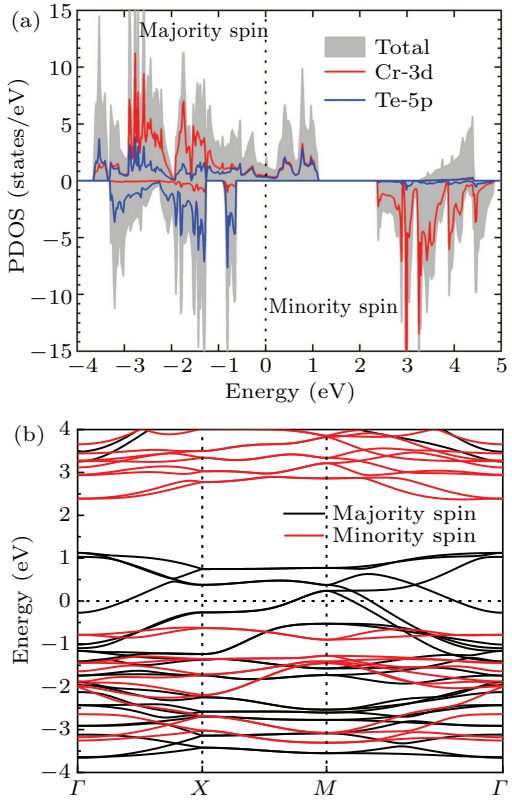


Fig. 6. (a) Density of states of the Cr-3d and Te-5p orbitals and (b) spin-resolved band structure of the $LiCrTe_2$ monolayer with $U_{\rm eff} = 3$ eV.

One of the important properties of ferromagnets is the Curie temperature $T_{\rm c}$. We adopted a classical Heisenberg model to estimate the $T_{\rm c}$ of the $LiCrTe_2$ monolayer. The Hamiltonian is shown as follow:

$$H = \frac{1}{2}J_1\sum_{\langle i,j\rangle}\boldsymbol{S}_i\cdot\boldsymbol{S}_j + \frac{1}{2}J_2\sum_{\langle\langle i,j\rangle\rangle}\boldsymbol{S}_i\cdot\boldsymbol{S}_j + \frac{1}{2}J_3\sum_{\langle\langle\langle i,j\rangle\rangle\rangle}\boldsymbol{S}_i\cdot\boldsymbol{S}_j + \frac{1}{2}J_4\sum_{\langle\langle\langle\langle i,j\rangle\rangle\rangle\rangle}\boldsymbol{S}_i\cdot\boldsymbol{S}_j + A\sum_i (S_i^z)^2,$$

where $\boldsymbol{S}_i$ represents the spin of Cr ion on the $i^{\rm th}$ site, while J_1, J_2, J_3 and J_4 denote the first-, second-, third-, and fourth-nearest exchange interaction parameters, respectively. The exchange interaction parameters can be extracted from the four ordered spin states method,[28–30] which is a general and efficient method to quantitatively describe spin–lattice coupling. A $4\times4\times1$ supercell (128 atoms) was used to calculate the interaction parameters J_1, J_2, J_3 and J_4. The results are listed in Table 1, in which the magnitude of $\boldsymbol{S}_i$ and $\boldsymbol{S}_j$ is set to 1. The negative J_1, with much larger absolute value than J_2, J_3 and J_4, supports the ferromagnetic ground state of $LiCrTe_2$. The magnetocrystalline anisotropy energy A is related to the energy differences between the in-plane and out-of-plane easy-axis obtained from the SOC calculations, i.e., $A = \frac{1}{N}\left(E_{i,z} - E_{i,x/y}\right) =$ 0.281 meV (0.407 meV for $U_{\rm eff} = 3.5$ eV and 0.608 meV for $U_{\rm eff} = 4$ eV) , where N is the number of magnetic atoms in the supercell.

By using Metropolis Monte Carlo (MC) simulations based on the above 2D Heisenberg model, we calculated

the Curie temperatures of the $LiCrTe_2$ monolayer by using a 100×100 supercell. Figure 7 shows the evolution of the normalized S and auto-correlation along with temperature. The Curie temperatures can be extracted from the peak of the auto-correlation, i.e., 1095 K, 695 K, and 640 K for $U_{\text{eff}} = 3$ eV, 3.5 eV, and 4 eV, respectively. For comparison, the T_c of the $LiCrTe_2$ monolayer with $P3m1$ space group is 285 K.[15,31]

Table 1. The exchange interaction parameters up to the fourth nearest neighbor and magnetocrystalline anisotropy energy in meV, in which the magnitudes of $\boldsymbol{S}_i$ and $\boldsymbol{S}_j$ are set to 1.

	J_1	J_2	J_3	J_4	A
$U_{\text{eff}} = 3.0$ eV	–138.18	–6.61	0.54	–1.99	0.281
$U_{\text{eff}} = 3.5$ eV	–116.06	–6.43	4.82	2.19	0.407
$U_{\text{eff}} = 4.0$ eV	–104.84	–3.40	5.96	0.28	0.620

The electronic properties of $LiCrTe_2$ monolayers are then investigated. The spin-polarized density of states and band structures are shown in Fig. 6. The density of states and band structures are overall similar as well for $U_{\text{eff}} = 3.5$ eV and 4 eV except for the small and predictable changes in the spin gap and exchange splitting. It can be found that the spin-majority bands cross the Fermi level, while the spin-minority bands have semiconducting characteristic. Such a band structure implies that $LiCrTe_2$ is an intrinsic half-metallic ferromagnet. In order to preserve the half-metallicity at room temperature, the spin gap needs to be wide enough to prevent thermally excited spin-flip transition. The calculated spin gap is 3.01 eV (3.10 eV for $U_{\text{eff}} = 3.5$ eV and 3.17 eV for $U_{\text{eff}} = 4$ eV) and it is wide enough to prevent spin leakage.

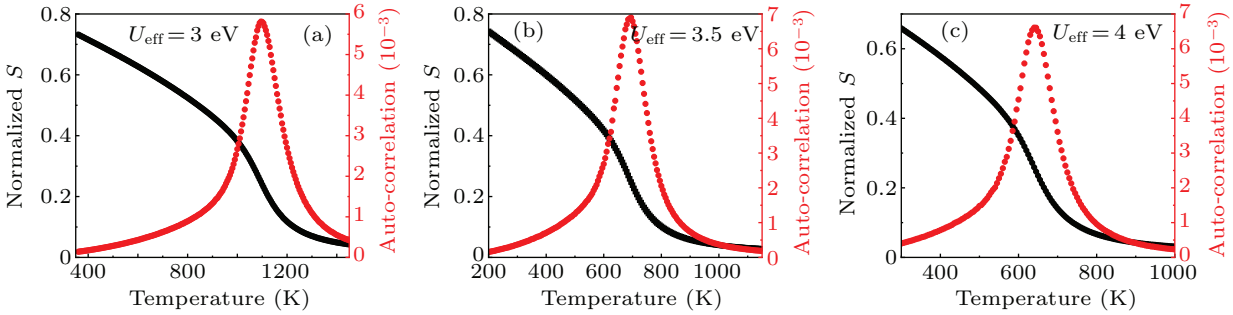


Fig. 7. The evolution of the normalized S and auto-correlation along with temperature for $U_{\text{eff}} = 3$ eV (a), 3.5 eV (b), and 4 eV (c).

The overlap between the Cr-3d and Te-5p orbitals in a large energy range (Fig. 6(a)) demonstrates the significant 3d–5p hybridization between them. And as shown in Fig. 5(b), the differential charge density of the $LiCrTe_2$ monolayer indicates that the electrons are transferred from Cr atoms to the middle zone of the Cr–Te bonds. This implies a covalent bonding nature between the Cr and Te atoms. Moreover, the projected crystal orbital Hamilton population (–pCOHP) analysis (Fig. 5(c)) shows that the anti-bonding states formed by the hybridized Te-5p and Cr-3d orbitals take a small part of area below the Fermi level, while the bonding states dominate the area below the Fermi level. This also indicates that a relatively strong chemical bond is formed between the Cr and Te atoms.

3.3. Effect of biaxial strains

Generally, the strain is a feasible method to adjust properties of various 2D materials.[32,33] We studied the changes of magnetic and electronic properties of monolayer $LiCrTe_2$ with biaxial strains ranging from -5% to $+5\%$. The applied biaxial strain is defined as

$$\varepsilon = \frac{a - a_0}{a_0}.$$

Here a and a_0 represent the lattice constants of strained and initial $LiCrTe_2$, respectively. The negative and positive ε denote biaxial compressive and tensile strains, respectively.

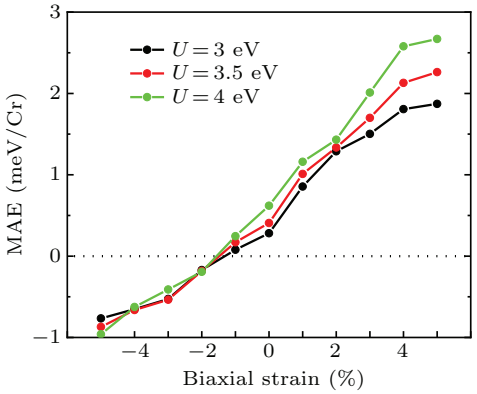


Fig. 8. The MAEs under biaxial strains ranging from -5% to $+5\%$. MAE < 0 and MAE > 0 represent the out-of-plane and in-plane magnetization, respectively.

The energy differences of the six AFM states with respect to the FM state, under the biaxial strains ranging from -5% to $+5\%$, are shown in Table 2. The $LiCrTe_2$ monolayer still keeps the FM ground state and the magnetic moments on Cr atoms are almost constant under the biaxial strains we studied. As shown in Fig. 8, the MAE of the $LiCrTe_2$ monolayer can be effectively adjusted by applying different strains. Both tensile and compressive strains can significantly increase the magnitude of MAE and the MAE can reach 1.79 meV/Cr (2.20 meV/Cr for $U_{\text{eff}} = 3.5$ eV and 2.61 meV/Cr for $U_{\text{eff}} = 4$ eV) at $+5\%$ biaxial strain. In particular, a transition from in-plane magnetization to out-of-plane magnetization occurs

when the compressive strain exceeds 1%. The Curie temperatures at different strains were further estimated by using Monte Carlo simulations. As shown in Fig. 9(c), the T_c is significantly higher than the room temperature for all situations we considered and the lowest estimated T_c is 869 K at +5% biaxial strain. When $U_{eff} = 3.5$ eV and 4 eV, the calculated Curie temperatures at +5% biaxial strain are 535 K and 694 K, respectively.

The half-metallicity is also maintained under the biaxial strains ranging from −5% to +5% for $U_{eff} = 3$ eV. However, for $U_{eff} = 3.5$ eV and $U_{eff} = 4$ eV, the metallic spin-majority channel opens a 61 meV and 101 meV direct gap at M point, respectively (Figs. 9(a) and 9(b)). This is believed to be caused by the band narrowing due to tensile strains together with the band shift by large U_{eff} parameters. On the other hand, the spin-minority gap increases gradually from 2.76 eV (2.84 eV for $U_{eff} = 3.5$ eV, 2.93 eV for $U_{eff} = 4$ eV) to 3.24 eV (3.32 eV for $U_{eff} = 3.5$ eV, 3.41 eV for $U_{eff} = 4$ eV), when the biaxial strains range from −5% to +5%. Meanwhile, the density of states near the Fermi level continues to decrease.

Table 2. The energy differences (in units of meV/Cr) of the AFM states with respect to the FM state under biaxial strains ranging from −5% to +5%. The U_{eff} is set to 3 eV.

	FM	AFM1	AFM2	AFM3	AFM4	AFM5	AFM6
–5%	0.00	184.82	191.07	206.66	235.43	219.54	494.28
–4%	0.00	180.96	197.99	213.48	239.29	239.32	493.37
–3%	0.00	184.19	201.82	216.43	239.99	247.20	491.74
–2%	0.00	185.16	206.63	209.34	243.42	256.45	494.71
–1%	0.00	184.28	207.81	214.49	244.47	263.25	493.53
0%	0.00	180.39	203.43	211.97	240.40	259.18	486.55
+1%	0.00	179.29	200.99	211.78	242.99	257.58	481.20
+2%	0.00	178.27	197.22	210.73	236.13	256.55	474.10
+3%	0.00	176.07	191.96	208.27	223.17	253.73	462.75
+4%	0.00	175.87	188.74	207.51	211.97	251.24	452.91
+5%	0.00	175.11	185.98	206.23	199.34	248.78	441.88

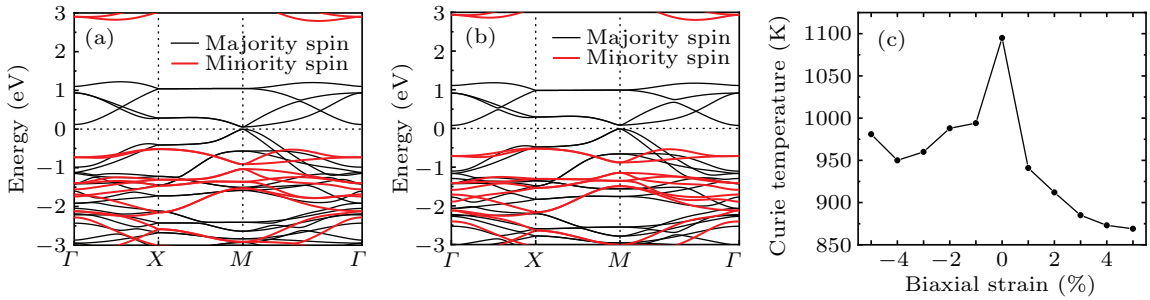


Fig. 9. Spin-resolved band structures of the $LiCrTe_2$ monolayer with (a) $U_{eff} = 3.5$ eV at +5% tensile strain and (b) $U_{eff} = 4$ eV at +4% tensile strain. (c) The variation of Curie temperatures with biaxial strains for $U_{eff} = 3$ eV.

4. Conclusion

In summary, by using first-principles electronic structure calculations, we proposed a new 2D half-metallic ferromagnet $LiCrTe_2$ monolayer. We systematically studied the $LiCrTe_2$ monolayer in terms of crystal structure, stability, electronic properties, and magnetic properties. We found that the $LiCrTe_2$ monolayer has a tetragonal structure with good thermal, dynamical, and mechanical stability. The $LiCrTe_2$ monolayer takes a ferromagnetic ground state with intrinsic easy-axis along x or y directions and the magnetic moment on each Cr atom is about 3.6 μ_B. The Curie temperatures estimated by using the statistical Monte Carlo (MC) simulations are above 600 K and significantly higher than the room temperature. The metallic spin-majority channel and the gapped spin-minority channel together demonstrate the half-metallicity nature of $LiCrTe_2$ and the sizeable gap in the spin-minority channel is critical for generating fully spin polarized carries. Under biaxial strains ranging from −5% to +5%, the ferromagnetism, wide spin gap, large magnetization, and high Curie temperature are all maintained well, while the magnetic anisotropy takes an in-plane easy-$x(y)$-axis to out-of-plane easy-z-axis transition when the compressive strain exceeds 1%. We expect that the discovery of $LiCrTe_2$ monolayer will provide a new option for exploring 2D magnetic materials and for spintronic applications in the future.

Acknowledgements

Project supported by the National Key R&D Program of China (Grant No. 2019YFA0308603) and the National Natural Science Foundation of China (Grant No. 11934020). Computational resources were provided by the Physical Laboratory of High Performance Computing at Renmin University of China.

References

[1] Hirohata A, Yamada K, Nakatani Y, Prejbeanu L, Diény B, Pirro P and Hillebrands B 2020 *J. Magnet. Magnet. Mater.* **509** 166711
[2] Li X and Yang J 2016 *Natl. Sci. Rev.* **3** 365
[3] Huang B, Clark G, Navarro-Moratalla E, Klein D R, Cheng R, Seyler K L, Zhong D, Schmidgall E, McGuire M A, Cobden D H, Yao W, Xiao D, Jarillo-Herrero P and Xu X 2016 *Nature* **546** 270
[4] Gong C, Li L, Li Z, Ji H, Stern A, Xia Y, Cao T, Bao W, Wang C, Wang Y, Qiu Z Q, Cava R J, Louie S G, Xia J and Zhang X 2017 *Nature* **546** 265
[5] Kuklin A V, Shostak S A and Kuzubov A A 2018 *J. Phys. Chem. Lett.* **9** 1422
[6] Ghosh A, Kar M, Majumder C and Sarkar P 2021 *Mat. Sci. Eng. B* **272** 115379
[7] Wang B, Zhang Y, Ma L, Wu Q, Guo Y, Zhang X and Wang J 2019 *Nanoscale* **11** 4204
[8] Kresse G and Furthmüller J 1996 *Comput. Mater. Sci.* **6** 15

[9] Kresse G and Furthmüller J 1996 *Phys. Rev. B* **54** 11169
[10] Perdew J P, Burke K and Ernzerhof M 1996 *Phys. Rev. Lett.* **77** 3865
[11] Blöchl P E 1994 *Phys. Rev. B* **50** 17953
[12] Kresse G and Joubert D 1999 *Phys. Rev. B* **59** 1758
[13] Monkhorst H J and Pack J D 1976 *Phys. Rev. B* **13** 5188
[14] Anisimov V I, Aryasetiawan F and Lichtenstein A I 1997 *J. Phys. Condens. Matter* **9** 767
[15] Xu W, Ali S, Jin Y, Wu X and Xu H 2020 *ACS Appl. Electron. Mater.* **2** 3853
[16] Togo A and Tanaka I 2015 *Scr. Mater.* **108** 1
[17] Nosé S 1984 *J. Chem. Phys.* **81** 511
[18] Kan M, Adhikari S and Sun Q 2014 *Phys. Chem. Chem. Phys.* **16** 4990
[19] Kan M, Zhou J, Sun Q, Kawazoe Y and Jena P 2013 *J. Phys. Chem. Lett.* **4** 3382
[20] Liu L, Ren X, Xie J, Cheng B, Liu W, An T, Qin H and Hu J 2019 *Appl. Surf. Sci.* **480** 300
[21] Millican J N, Phelan D, Thomas E L, Leão J B and Carpenter E 2009 *Solid State Commun.* **149** 707
[22] Wang V, Tang G, Wang R T, Liu Y C, Mizuseki H, Kawazoe Y, Nara J and Geng W T 2018 *arXiv* 1806.04285
[23] Booth T J, Blake P, Nair R R, Jiang D, Hill E W, Bangert U, Bleloch A, Gass M, Novoselov K S, Katsnelson M I and Geim A K 2008 *Nano Lett.* **8** 2442
[24] Liu J, Sun Q, Kawazoe Y and Jena P 2016 *Phys. Chem. Chem. Phys.* **18** 8777
[25] Li X and Yang J 2014 *J. Mater. Chem. C* **2** 7071
[26] Jiang X, Liu Q, Xing J, Liu N, Guo Y, Liu Z and Zhao J 2021 *Appl. Phys. Rev.* **8** 031305
[27] Daalderop G H O, Kelly P J and Schuurmans M F H 1990 *Phys. Rev. B* **41** 11919
[28] Ma F, Lu Z Y and Xiang T 2008 *Phys. Rev. B* **78** 224517
[29] Ma F, Ji W, Hu J, Lu Z Y and Xiang T 2009 *Phys. Rev. Lett.* **102** 177003
[30] Xiang H J, Kan E J, Wei S H, Whangbo M H and Gong X G 2011 *Phys. Rev. B* **84** 224429
[31] Li, P, Cui Q, Ga Y, Liang J and Yang H 2022 *Phys. Rev. B* **106** 24419
[32] Zhou Y, Wang Z, Yang P, Zu X, Yang L, Sun X and Gao F 2012 *ACS Nano* **6** 9727
[33] Joe M, Lee H, Alyörük M M, Lee J, Kim S Y, Lee C and Lee J H 2017 *J. Phys. Condens. Matter* **29** 405801